Proc. Natl. Acad. Sci. USA
Vol. 90, pp. 11757–11761, December 1993
Biophysics

The accessory bacteriochlorophyll: A real electron carrier in primary photosynthesis

(*Rhodobacter sphaeroides*/primary photoreaction/reaction center/femtosecond spectroscopy)

T. ARLT†, S. SCHMIDT†, W. KAISER†, C. LAUTERWASSER‡, M. MEYER§, H. SCHEER§, AND W. ZINTH‡

†Technische Universität München, Physik Department E 11, 85748 Garching/Munich, Federal Republic of Germany; ‡Ludwig-Maximilians-Universität München, Institut für Medizinische Optik, 80797 Munich, Federal Republic of Germany; and §Ludwig-Maximilians-Universität München, Botanisches Institut, 80638 Munich, Federal Republic of Germany

Contributed by W. Kaiser, September 7, 1993

ABSTRACT **The primary electron transfer in reaction centers of *Rhodobacter sphaeroides* is studied by subpicosecond absorption spectroscopy with polarized light in the spectral range of 920–1040 nm. Here the bacteriochlorophyll anion radical has an absorption band while the other pigments of the reaction center have vanishing ground-state absorption. The transient absorption data exhibit a pronounced 0.9-ps kinetic component which shows a strong dichroism. Evaluation of the data yields an angle between the transition moments of the special pair and the species related with the 0.9-ps kinetic component of 26 ± 8°. This angle compares favorably with the value of 29° expected for the reduced accessory bacteriochlorophyll. Extensive transient absorbance data are fully consistent with a stepwise electron transfer via the accessory bacteriochlorophyll.**

In the primary processes of bacterial photosynthesis, absorbed light energy is stored via an electron transfer within the reaction center (RC). While the molecular structure of two bacterial reaction centers has been known for a number of years (1–3), the detailed molecular mechanism of the electron transfer is still the subject of intense investigations (4–20). There is general agreement that the first electron transfer process starts at a pair of bacteriochlorophyll (BChl) molecules—the special pair P—which acts as the primary donor. The special pair is excited by energy transfer from antenna molecules or by direct light absorption. The excited electronic state P* exists for ≈3 ps. With the same time constant, absorption features appear which have been assigned to a RC containing the reduced bacteriopheophytin (BPhe), H_A^-, on the A branch. After ≈200 ps the electron is transferred to the quinone Q_A in a final picosecond process. In addition to these well-established transfer steps, transient absorption data presented by several investigators (5–8, 12, 17, 20) indicate a third kinetic process characterized by a very short time constant of 0.9 ps and 0.65 ps for RCs of *Rhodobacter sphaeroides* and *Rhodopseudomonas viridis*, respectively. This kinetic component has significant amplitudes only at spectral positions where the BChl or its anion radical shows strong absorption. To be detailed: The subpicosecond component is clearly resolved in the BChl Q_y and Q_x absorption bands and in the BChl anion band around 650 nm (5, 7, 8). The results were consistently described by a model where the electron is transferred from the special pair to the BPhe via the accessory BChl B_A, forming a short-lived BChl anion B_A^-. The two-step electron transfer may be written in the form

$$P^* \xrightarrow{3\ ps} P^+B_A^- \underset{0.6\ ps}{\overset{0.9\ ps}{\rightleftharpoons}} P^+H_A^- \xrightarrow{200\ ps} P^+Q_A^-. \qquad [1]$$

A frequent objection to the transfer model 1 is based on the fact that the spectral regions where the subpicosecond component is seen most clearly are somewhat congested. Furthermore, in ref. 6 the fast component was interpreted as the result of a structural heterogeneity. Recent emission experiments added further complexity to the situation: the decay of P* was found to be non-monoexponential (11, 18) and could be fitted, in a first-order approximation, by a biexponential function with decay times of 2.3 ps and 7 ps (11). This non-monoexponentiality of the decay of P* found for *Rb. sphaeroides* fitted well to earlier observations on RCs of *Chloroflexus aurantiacus* (21, 22). More recently, short-lived oscillations were observed in the transient absorption spectroscopy of RCs at low temperatures (9, 10). In active RCs under physiological condition—i.e., at room temperature—these oscillations were not detected.

In this paper we present experimental data demonstrating the appearance of the subpicosecond component in the spectral range of 1000 nm, where neither the special pair P nor BChl, BPhe, or BPhe anion radicals have absorption bands. The subpicosecond component in this range can be related directly to a BChl anion radical. Additional strong support comes from transient dichroic measurements where the observed direction of the transition moment of the short-lived intermediate is compared with calculations based on the structure of the RCs.

MATERIALS AND METHODS

RCs were isolated from the carotenoid-less strain R26.1 of *Rb. sphaeroides* (5). The transient absorption measurements were performed at room temperature in cuvettes with 1-mm pathlength. The concentration of the sample was adjusted to OD 20 cm^{-1} at 860 nm. The excited volume was exchanged between two laser shots by stirring. For the time-resolved excite-and-probe experiments, we worked with a femtosecond spectrometer based on a colliding pulse-mode-locked (CPM) dye laser. Generation and amplification of the femtosecond pulses are described elsewhere (20). The salient parameters of the system are as follows: repetition rate, 50 Hz; wavelength of the pump pulses, λ_{exc} = 865 nm; excitation of <20% of the RCs in the irradiated volume. Probing pulses are produced by femtosecond continuum generation. They have a spectral width of 15 nm. The instrumental response function—i.e., the cross-correlation between excitation and probing pulses—has a temporal width of 250 fs. The two beams cross in the sample at an angle of 8°. If not stated otherwise, polarization of exciting and probing pulses was parallel.

The time-resolved absorption data (Figs. 1, 2, and 4) were modeled by sums of exponentials convoluted with the instru-

The publication costs of this article were defrayed in part by page charge payment. This article must therefore be hereby marked "*advertisement*" in accordance with 18 U.S.C. §1734 solely to indicate this fact.

Abbreviations: RC, reaction center; BChl, bacteriochlorophyll; BPhe, bacteriopheophytin.

mental response function $K(t)$. The mathematical description of the transmission $T(t)$ or of the transient absorbance changes $\Delta A(t) = -\log[T(t)/T(t = -\infty)]$ was performed by a system of rate equations which provide a set of amplitudes a_j and decay constants k_j (or decay times $\tau_j = 1/k_j$):

$$\Delta A(t, \lambda_{pr}) = \int_0^\infty \sum_{j=1}^{n} a_j(\lambda_{pr}) \cdot \exp(-t' \cdot k_j) \cdot K(t - t')dt'.$$

For a specific reaction model one is able to calculate spectra of difference cross section $\Delta\sigma_i(\lambda_{pr}) = \sigma_i(\lambda_{pr}) - \sigma_0(\lambda_{pr})$ of the intermediates from the amplitudes a_j (see refs. 7 and 23).

RESULTS

Time-Resolved Spectral Data. Transient absorption data were collected in the spectral range between 920 nm and 1040 nm, where ground-state pigments of the RC do not absorb. From the potential intermediates only the anion radical of BChl, B_A^-, is known to have an absorption band *in vitro* around 1000 nm (reproduced in Fig. 5*b*, dashed line) (24, 25). Data of our transient absorption experiments taken over a wide time range are presented in Figs. 1 and 2. At 940 nm (Fig. 1), in the short-wavelength end of the investigated regime, an apparent strong decrease of absorption at delay time zero is observed. This first absorption decrease recovers with a time constant of several picoseconds to an enhanced weak absorption. Since there is no ground-state absorption at 940 nm, the initial apparent absorbance decrease must be due to amplification (gain) of the probe pulse via stimulated emission from the excited electronic level P*. For longer probing

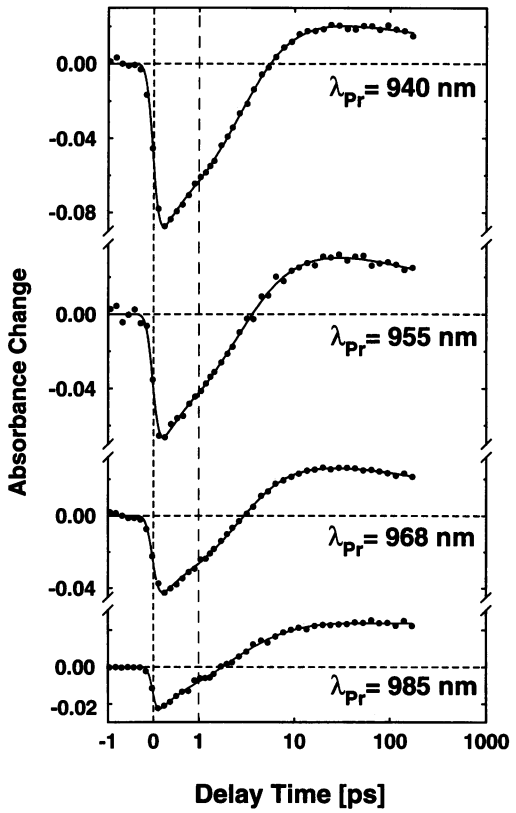

FIG. 1. Changes of absorbance after excitation at λ_{exc} = 865 nm (points) for RCs of *Rb. sphaeroides* R26.1 at room temperature. The curves (solid lines) were calculated with five time constants: 0.9 ps, 2.3 ps, 7.0 ps, 200 ps, and infinity [amplitude ratio a(7 ps)/a(2.3 ps) = 0.3]. Note the linear scale for the delay times of <1 ps and the logarithmic scale at later delay times. λ_{Pr}, probing wavelength.

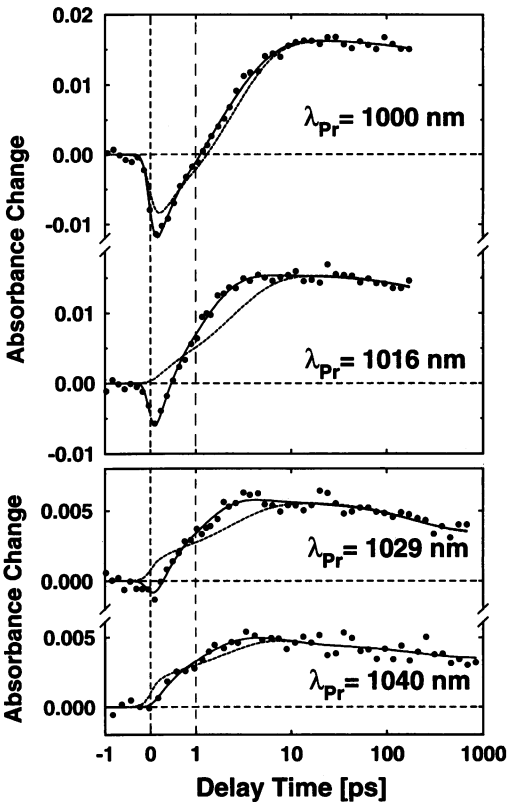

FIG. 2. Change of absorbance as in Fig. 1. The solid curves were calculated with five time constants, 0.9 ps, 2.3 ps, 7 ps, 200 ps, and infinity, while the broken curves were calculated without the 0.9-ps component. Note the different scale used for the absorbance changes in the lower part.

wavelengths the stimulated emission (gain) decreases and a faster absorption transient appears. This new transient is clearly seen for probing wavelengths (λ_{pr}) of 1000 nm and 1016 nm (Fig. 2). A three-component fit with the time constants 2.3, 7, and 200 ps (dashed lines) is not adequate to account for the data points. An additional faster kinetic component with the time constant 0.9 ps (solid lines) is required to simulate the experimental data. At still longer probing wavelengths (1040 nm) the gain around time zero has disappeared. A careful inspection of the signal traces (1029 nm, 1040 nm), where time zero was determined in an independent experiment with a precision of better than 50 fs, shows a substantial mismatch between data points and the three-component fit.

In Fig. 3 the amplitudes related to the various kinetic components are plotted as a function of probing wavelength. The amplitudes of the 2.3- and 7-ps kinetic component are approximately proportional to each other with a(7 ps)/a(2.3 ps) $\approx$ 0.3. This amplitude ratio is close to the value of 0.25 found in previous time-resolved emission experiments (11). Both amplitudes decrease continuously for longer wavelengths and vanish for λ_{pr} > 1016 nm. The amplitude of the 0.9-ps kinetic component a(0.9 ps) is very weak at shorter wavelengths in the gain region. At longer wavelengths the amplitude a(0.9 ps) becomes substantial, with its maximum value around 1016 nm. It should be noted in this context that the subpicosecond component contributes 70% to the total signal amplitude at 1016 nm. In other words, the 0.9-ps component appears as a strong signal readily seen in our measurements and far above any noise background. The 200-ps component related to the electron transfer between H_A^- and Q_A is weak at all probing wavelengths. This observation is expected, since H_A^- has negligible absorption in this

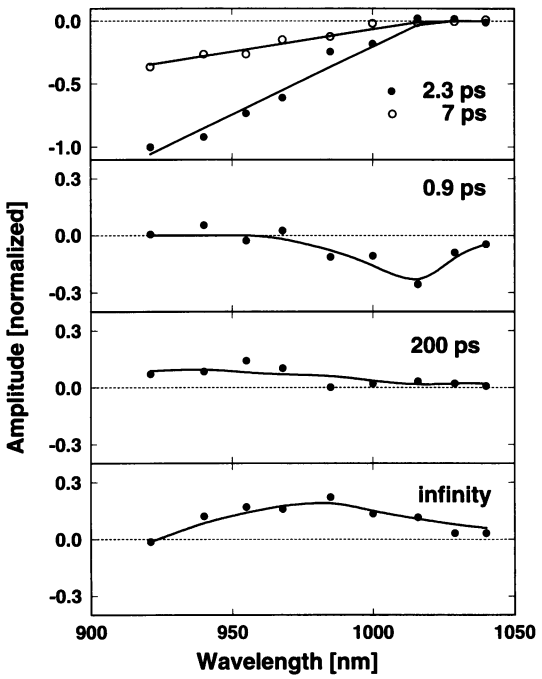

FIG. 3. Spectra of amplitudes of the five kinetic components obtained by evaluation of the data of Figs. 1 and 2 for various probing wavelengths.

wavelength range. As all RCs reach the final state $P^+Q_A^-$ at very late delay times, the amplitude "infinity" shown at the bottom of Fig. 3 corresponds to the spectrum of $P^+Q_A^-$. It displays a broad peak around 980 nm representing the absorption of the cation P^+ of the special pair (26). We repeat that Q_A, Q_A^-, and P do not absorb in the investigated spectral region. The spectra of the other intermediates are discussed below.

Time-Resolved Dichroic Data. The absence of ground-state absorption of the RC in the spectral range investigated here allows a determination of the direction of dipole moments by dichroic experiments. A probing wavelength of 998 nm was chosen (Fig. 4), where stimulated emission and the 0.9-ps component are of approximately equal magnitude. Data taken with parallel polarization between excitation and probe pulses (points) have the same transient behavior as shown in Fig. 2. With perpendicular polarization (triangles) the transient absorption curve is changed in shape and reduced in magnitude. At early times an absorbance ratio $\Delta A_\parallel/\Delta A_\perp \approx 3$ is found, while at late delay times (>200 ps) this ratio is $\Delta A_\parallel/\Delta A_\perp \approx 2.1$. These numbers determine the directions of the transition dipole moments of the species present at early

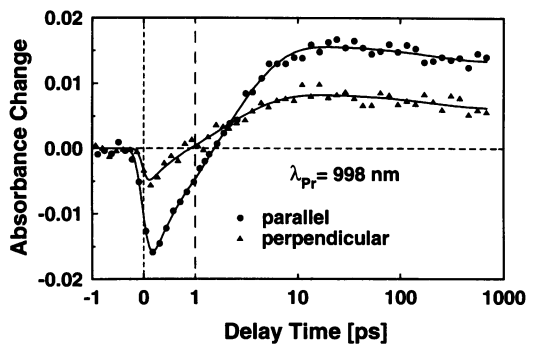

FIG. 4. Time-resolved absorption change taken at λ_{pr} = 998 nm for RCs of *Rb. sphaeroides*. Pump and probe pulses are parallel (●) and perpendicular (▲) polarized. The curves (solid lines) were calculated with the five time constants of Fig. 2.

Table 1. Amplitudes of the exponential functions used to model the data at a probe wavelength of 998 nm

	a(2.3 ps)	*a*(7 ps)	*a*(0.9 ps)	*a*(200 ps)	*a*(∞)
∥	−1.68	−0.58	−1.46	0.32	1.30
⊥	−0.74	−0.22	−0.61	0.27	0.61

and late times relative to the direction of the absorption dipole moment of P. For P* at the beginning and P^+ around 500 ps one finds the corresponding angles of approximately 0° and 27°, respectively. Modeling the dichroic data with exponential functions using the time constants discussed above, one obtains the amplitudes shown in Table 1. For specific reaction models the amplitudes can be used to calculate the direction of the transition moments of other intermediates.

DISCUSSION

The spectral range investigated in this paper allows a ready interpretation of the experimental data. There is no interference from ground-state absorptions or from electrochromic shifts or from absorption of the BPhe anion.

Due to the apparent absence of coherence effects at room temperature¶ it is justified to work with a rate equation system as a first-order description of the electron transfer. The observation of two time constants (2.3 and 7 ps) in emission and absorption experiments related to the decay of P* requires an extension of the reaction picture. As a possible explanation of the non-monoexponential decay, a "parking" state (11) or a distribution in the difference of the Gibbs free energy ΔG (18) has been suggested. These models do not yield significant differences for the shapes of the transient spectra presented in the following. The model we use involves a parallel reaction with two substates of P*. The dominant fraction (77%) of the excited RCs have a fast decay time constant of 2.3 ps (reaction model 2), the remaining 23% decay with 7 ps (reaction model 3).

$$P^* \xrightarrow{2.3\ ps} P^+B_A^- \xrightarrow{0.9\ ps} P^+H_A^- \xrightarrow{200\ ps} P^+Q_A^- \qquad [2]$$

$$P^* \xrightarrow{7\ ps} P^+B_A^- \xrightarrow{0.9\ ps} P^+H_A^- \xrightarrow{200\ ps} P^+Q_A^-. \qquad [3]$$

In our model the spectral properties of the two fractions of reaction centers are considered to be the same. With these assumptions one calculates the spectra of the intermediates shown in Fig. 5 without free parameters. The emission spectrum of P* is proportional to the sum of all measured amplitudes a_j (7). It decreases continuously with wavelength (Fig. 5*a*). The pure B_A^- spectrum (Fig. 5*b*) is obtained by taking the difference between the spectra of $P^+B_A^-$ and P^+. $\Delta\sigma(B_A^-)$ has a peak around 1010 nm and a broad shoulder in the range 920–970 nm.‖ Qualitatively it agrees well with the spectrum of the BChl anion radical in solution (25) (dashed line in Fig. 5*b*). There is a spectral shift of ≈20 nm, in agreement with similar spectral shifts known for the other bands of B. The absorption cross section of B_A^- was calculated from the absolute cross section of P in ref. 27 and the difference cross-section spectrum (Fig. 5). Considering the small transient population of B_A^- discussed previously (5), we

¶In the data presented here no oscillations are found in spite of sufficient time resolution. In fact, oscillations at room temperatures have never been seen even in the photosynthetically inactive mutant RC D_{LL} (19).

‖In a stepwise electron transfer model, where the second time constant (0.9 ps) is shorter than the first one, a negative amplitude *a*(0.9 ps) corresponds to an absorption of the related intermediate which is more positive than the absorption of the first state (5, 23).

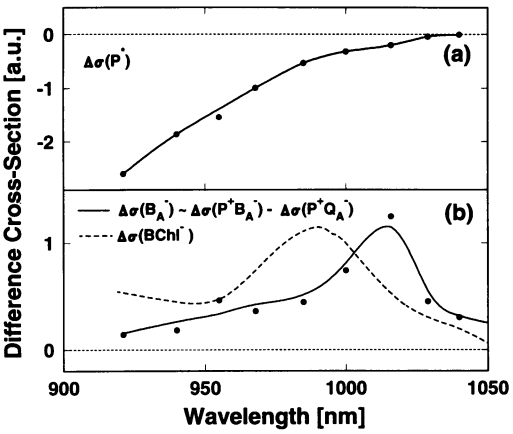

FIG. 5. Spectra of difference cross sections $\Delta\sigma$ of the two intermediates P* (*a*) and B_A^- (*b*). The points (●) were calculated from the time-resolved absorption data, by assuming the sequential two-step model of Eqs. 2 and 3. The solid lines were drawn to guide the eye. The dashed line in *b* represents the absorption spectrum of $BChl^-$ in dimethylformamide from Fajer *et al.* (25). a.u., Arbitrary units.

find an extinction coefficient which agrees within 20% with the value in solution (25).

Additional support for the presented reaction model comes from the observed induced photodichroism, which allows a determination of the angle α between the direction of the transition dipole moments of the intermediates and the direction of the special pair. For a ratio of cross sections $s = \Delta\sigma_\parallel/\Delta\sigma_\perp$ of a specific state one calculates the angle α (28):

$$\alpha = \arccos\left[\left(\frac{2s-1}{s+2}\right)^{1/2}\right]. \qquad [4]$$

Angles α for P*, P^+, and B^- are summarized in Table 2. The $\Delta\sigma$ values were calculated with the time constants of reaction models 2 and 3 and the amplitudes of Table 1 (7, 23). The transition dipoles of P* and P are approximately parallel to each other, whereas the dipole of P^+ exhibits an angle α = 27°. Most important for the present paper is the orientation of B_A^-. The evaluation of our data provides a number of α = 26° ± 8°. It has been shown (29) that the transition moments of the long-wavelength transition of B_A^- are parallel to the Q_y direction which points from the nitrogen at ring 1 to the nitrogen at ring 3. Taking advantage of the known x-ray structure of the RCs, one can predict an angle of α = 29° between the Q_y transitions of P and B_A^-, which agrees well with the experimental result.

The polarized absorption data allow a critical test for other reaction models—e.g. for the one-step model with a direct electron transfer from P to $P^+H_A^-$ via a superexchange mechanism. In this model it is necessary to assign the 0.9-ps component to a fast-decaying fraction of P*, which leads to intrinsic contradictions: the resulting dichroic ratio $\Delta\sigma_\parallel/\Delta\sigma_\perp$ of considerably more than 3 for this component is not allowed.

Table 2. Calculated difference cross-sections ($\Delta\sigma$) at 998 nm and angles (α) between the direction of the transition dipole moments of the intermediates and the absorption dipole moment of the Q_y transition of the special pair

	P*	P^+	B_A^-
$\Delta\sigma_\parallel$, 10^{-17} cm^2	−3.10	1.92	4.60
$\Delta\sigma_\perp$, 10^{-17} cm^2	−1.03	0.90	2.10
α, degrees	0–8	27 ± 15	26 ± 8

Conclusions. Transient absorption data on RCs of *Rb. sphaeroides* R26.1 at room temperature in the spectral range between 920 and 1040 nm show convincingly the existence of the subpicosecond (0.9-ps) kinetic component. The data allow (from spectrally resolved as well as from dichroic data) the assignment of this component to a transiently populated radical pair state $P^+B_A^-$. The experimental results supplement previously published data. For *all* spectral positions in the visible and near infrared—i.e., between 500 nm and 1040 nm—the transient data are in accordance with a picture of an intermediate $P^+B_A^-$ in a stepwise reaction model. This agreement gives strong evidence—if not proof—for a primary electron transfer involving the accessory BChl as a real electron carrier.

This work was supported by the Deutsche Forschungsgemeinschaft (SFB 143).

1. Deisenhofer, J., Epp, O., Miki, K., Huber, R. & Michel, H. (1985) *Nature (London)* **318**, 618–624.
2. Allen, J., Feher, G., Yeates, T. O., Komiya, H. & Rees, D. C. (1987) *Proc. Natl. Acad. Sci. USA* **84**, 5730–5734.
3. Arnoux, B., Ducruix, A., Reiss-Housson, F., Lutz, M., Norris, J. R., Schiffer, M. & Chang, C. H. (1989) *FEBS Lett.* **258**, 47–50.
4. Martin, J.-L., Breton, J., Hoff, A. J., Migus, A. & Antonetti, A. (1986) *Proc. Natl. Acad. Sci. USA* **83**, 957–961.
5. Holzapfel, W., Finkele, U., Kaiser, W., Oesterhelt, D., Scheer, H., Stilz, H. U. & Zinth, W. (1989) *Chem. Phys. Lett.* **160**, 1–7.
6. Kirmaier, C. & Holten, D. (1990) *Proc. Natl. Acad. Sci. USA* **87**, 3552–3556.
7. Holzapfel, W., Finkele, U., Kaiser, W., Oesterhelt, D., Scheer, H., Stilz, H. U. & Zinth, W. (1990) *Proc. Natl. Acad. Sci. USA* **87**, 5168–5172.
8. Dressler, K., Umlauf, E., Schmidt, S., Hamm, P., Zinth, W., Buchanan, S. & Michel, H. (1991) *Chem. Phys. Lett.* **183**, 270–276.
9. Vos, M. H., Lambry, J.-C., Robles, S. J., Youvan, D. C., Breton, J. & Martin, J.-L. (1991) *Proc. Natl. Acad. Sci. USA* **88**, 8885–8889.
10. Vos, M. H., Lambry, J.-C., Robles, S. J., Youvan, D. C., Breton, J. & Martin, J.-L. (1992) *Proc. Natl. Acad. Sci. USA* **89**, 613–617.
11. Hamm, P., Gray, K. A., Oesterhelt, D., Feick, R., Scheer, H. & Zinth, W. (1993) *Biochim. Biophys. Acta* **1142**, 99–105.
12. Chan, C.-K., DiMagno, T. J., Chen, L. X.-Q., Norris, J. R. & Fleming, G. R. (1991) *Proc. Natl. Acad. Sci. USA* **88**, 11202–11206.
13. Reddy, N. R. S., Lyle, P. A. & Small, G. J. (1992) *Photosynth. Res.* **31**, 167–194.
14. Marcus, R. A. (1987) *Chem. Phys. Lett.* **133**, 471–477.
15. Bixon, M., Jortner, J. & Michel-Beyerle, M. E. (1991) *Biochim. Biophys. Acta* **1056**, 301–315.
16. Michel-Beyerle, M. E., Plato, M., Deisenhofer, J., Michel, H., Bixon, M. & Jortner, J. (1988) *Biochim. Biophys. Acta* **932**, 52–70.
17. Lauterwasser, C., Finkele, U., Scheer, H. & Zinth, W. (1991) *Chem. Phys. Lett.* **183**, 471–477.
18. Du, M., Rosenthal, S. J., Xie, X., DiMagno, T. J., Schmidt, M., Hanson, D. K., Schiffer, M., Norris, J. R. & Fleming, G. R. (1992) *Proc. Natl. Acad. Sci. USA* **89**, 8517–8521.
19. Vos, M. H., Rappaport, F., Lambry, J.-C., Breton, J. & Martin, J.-L. (1993) *Nature (London)* **363**, 320–325.
20. Schmidt, S., Arlt, T., Hamm, P., Lauterwasser, C., Finkele, U., Drews, G. & Zinth, W. (1993) *Biochim. Biophys. Acta* **1144**, 385–390.
21. Martin, J. L., Lambry, J. C., Ashokkumar, M., Michel-Beyerle, M. E., Feick, R. & Breton, J. (1990) in *Ultrafast Phenomena VII*, Springer Series in Chemical Physics, eds. Harris, C. B., Ippen, E. P., Mourou, G. A. & Zewail, A. H. (Springer, Berlin), Vol. 53, pp. 524–528.
22. Becker, M., Nagarajan, V., Middendorf, D., Parson, W. W., Martin, J. E. & Blankenship, R. E. (1991) *Biochim. Biophys. Acta* **1057**, 299–312.
23. Finkele, U., Dressler, K., Lauterwasser, C. & Zinth, W. (1990)

in *Reaction Centers of Photosynthetic Bacteria*, Springer Series in Biophysics, ed. Michel-Beyerle, M. E. (Springer, Berlin), Vol. 6, pp. 127–134.
24. Fajer, J. (1973) *J. Am. Chem. Soc.* **95**, 2739–2741.
25. Fajer, J., Brune, D. C., Davis, M. S., Forman, A. & Spaulding, L. D. (1975) *Proc. Natl. Acad. Sci. USA* **72**, 4956–4960.
26. Parson, W. W., Nabedryk, E. & Breton, J. (1992) in *The Photosynthetic Bacterial Reaction Center II*, eds. Breton, J. & Verméglio, A. (Plenum, New York), pp. 79–88.
27. Straley, S. C., Parson, W. W., Mauzerall, D. C. & Clayton, R. K. (1973) *Biochim. Biophys. Acta* **305**, 597–609.
28. Vermeglio, A., Breton, J., Paillotin, G. & Cogdell, R. (1978) *Biochim. Biophys. Acta* **501**, 514–530.
29. Clayton, R. K. (1980) in *Photosynthesis: Physical Mechanisms and Chemical Patterns*, ed. Clayton, R. K. (Cambridge Univ. Press, Cambridge, U.K.), pp. 146–162.